Article

Different Fates of Alzheimer's Disease Amyloid-beta Fibrils Remodeled by Biocompatible Small Molecules

Jacob A. Irwin, H. Edward Wong, and Inchan Kwon

Biomacromolecules, **Just Accepted Manuscript** • DOI: 10.1021/bm3016994 • Publication Date (Web): 19 Nov 2012

Different Fates of Alzheimer's Disease Amyloid-beta Fibrils Remodeled by Biocompatible Small Molecules

*Jacob A. Irwin,[1] H. Edward Wong,[1] Inchan Kwon[1,2,]**

Department of Chemical Engineering[1] and Institutes on Aging[2]

University of Virginia,

Charlottesville, Virginia 22904

ik4t@virginia.edu

* To whom correspondence should be addressed. E-mail: ik4t@virginia.edu, telephone number: 434-243-1822, fax number: 434-982-2658

Abstract

Amyloid fibrils implicated in numerous human diseases are thermodynamically very stable. Stringent conditions that would not be possible in a physiological environment are often required to disrupt the stable fibrils. Recently, there is increasing evidence that small molecules can remodel amyloid fibrils in a physiologically relevant manner. In order to investigate possible fibril remodeling mechanisms using this approach, we performed comparative studies on the structural features of the different amyloid-beta (Aβ) aggregates remodeled from Aβ fibrils by three biocompatible small molecules: methylene blue; brilliant blue G; and erythrosine B. Combined with CD, immuno-blotting, TEM, and AFM results, it was found that brilliant blue G- and erythrosine B-treatment generate fragmented Aβ fibrils and protofibrils, respectively. In contrast, incubation of the Aβ fibrils with methylene blue perturbs fibrillar structure leading to amorphous Aβ aggregates. Our findings provide insights on the molecular mechanism of amyloid fibril formation and remodeling and also illustrate the possibility of controlled changes in biomolecule nanostructures.

Keywords: amyloid-beta, amyloid fibril, secondary structure, circular dichroism, erythrosine B, brilliant blue

Introduction

The amyloid fibril is one of the most biologically important protein structures due to its implication in numerous neurodegenerative diseases, such as Alzheimer's disease (AD), Parkinson's disease (PD), and prion disease.[1-4] Intrinsically disordered monomeric peptide and protein, such as amyloid-beta (Aβ) peptide and α-synuclein, aggregate to form prefibrillar or fibrillar oligomers, leading to amyloid fibrils with cross-stacked β-sheet structure.[5]

Since amyloid fibrils are thermodynamically very stable,[6] it has been generally accepted that reversing the preformed amyloid fibrils into smaller intermediates does not occur spontaneously. Therefore, several strategies employing physiological and non-physiological conditions have been investigated to break, disrupt, and/or destabilize amyloid fibrils (for a recent comprehensive review on this subject, see Ref [7]). As a non-physiological condition, physical energy has been applied to break down mature fibrils. Ultrasonication has been found to fragment preformed amyloid fibrils into shorter fibril fragments that can be used to template further fibril formation.[8] Additionally, high temperatures (above 100 ◦C) have been found to disrupt the strength of hydrogen-bond networks which are crucial for the rigid fibril structure, leading ultimately to destruction of fibril structure.[7, 9] Because charge is a very important factor in fibril structure stability, drastic changes in pH or salt levels can lead to fibril destruction. Specifically, pH levels above 8 have been shown to lead to complete loss of β-sheet interactions.[10] Similarly, the addition of strong ionic liquids can block the electrostatic repulsion forces needed to hold together neighboring protofibrils during the fibril twisting process.[11] Finally, the introduction of denaturants (such as guanidine hydrochloride) or co-solvents (such as hexafluoroisopropanol (HFIP) and dimethylsufoxide) have also been shown to strongly destabilize preformed amyloid fibrils.[12, 13] Water-ethanol solutions have been found to have a lesser effect over shorter time periods (< 1 day), but still converted mature fibrils into shorter, worm-like fibrils over a period of several weeks.[14]

Besides these non-physiological conditions, recent findings demonstrate that preformed amyloid fibrils can be destabilized by endogenous or exogenous compounds in physiological conditions. L-

dihydroxy-phenylalanine (L-DOPA), an endogenous precursor of dopamine, disaggregated the amyloid fibrils formed in the mouse brain generating toxic smaller aggregates,[15] illustrating the possibility that insoluble amyloid fibrils are a source of toxic soluble oligomers/protofibrils[16] by interacting with destabilizing chemical compounds. Surfactants (such as Triton X-100 and sodium dodecyl sulfate) have been used to destabilize fibrils through the promotion of molecular orientations with unfavorable energy. An interesting example of the interaction of surfactants with mature amyloid fibrils is the work by Ruhs, et al., employing sulfonic-acid-terminated PEG.[17] The strong electrostatic interactions between the PEG and fibrils reduced the entropy of the native amyloid fibril structure, resulting in its conversion to an amorphous, globular ending structure. It was also reported that several small molecules often introduced into human body (exogenous small molecules), such as doxycycline, epigallocatechin gallate, rifampicin, and dequalinium, destabilize preformed amyloid fibrils.[18-20] Despite the increasing number of cases demonstrating that amyloid fibrils can be destabilized by small molecules, the underlying molecular mechanisms still remain largely unclear.[7] In particular, different fates of the destabilized amyloid fibrils have not yet been extensively investigated. Considering that endogenous and exogenous compounds can directly destabilize amyloid fibrils present in the human body, investigating the different fates of the destabilized amyloid fibrils will provide insights on molecule-level pathological mechanism of amyloid fibrils as well as small molecule-induced structural conversion of biomacromolecules.

Therefore, we performed comparative studies on the structural features of the different Aβ aggregates converted from amyloid fibrils destabilized by three exogenous biocompatible small molecules. We chose three small molecules, methylene blue (MB), brilliant blue G (BBG), and erythrosine B (ER) (Figure 1), due to their favorable features for our studies. First, these three molecules are effective modulators of Aβ aggregation and cytotoxicity. We recently reported that red food dye (ER) and the blue food dye analog (BBG) are novel small-molecule modulators of Aβ40 aggregation and effectively eliminate Aβ-associated cytotoxicity by promoting non-toxic Aβ aggregate formation but reducing toxic Aβ aggregate formation.[21, 22] MB has also been shown to modulate Aβ42 aggregation and cytotoxicity by promoting less toxic amyloid fibril formation but preventing the formation of very toxic

pre-fibrillar oligomers.[23, 24] Therefore, we expect that these three molecules will interact with Aβ40 fibrils despite the lack of previous evidence. Second, MB, BBG, and ER are structurally quite distinct, representing phenothiazine, triphenylmethane, and xanthene benzoate groups, respectively. Therefore, these three molecules most likely have different interaction modes on Aβ40 fibrils. Third, these three molecules have good potential for therapeutic application since they are safe, biocompatible, and potentially blood-brain barrier permeable.[25-37] MB has already been shown to have a wide variety of medicinal applications, including treatment of malaria and cancer.[38-40] Furthermore, the Phase II clinical trials of MB on AD demonstrated promising results.[41] BBG expedited the recovery after spinal cord injury and conferred neuroprotection to the brain by mitigating AD and multiple sclerosis symptoms.[33, 36, 37] ER is a Food and Drug Administration-approved red food coloring dye. A daily dose up to 60 mg/kg of ER is non-toxic to humans.[30] These three compounds are either being taken or might be taken in the future by humans. Since testing small molecules in vivo is not trivial, in vitro studies on the effects of these three molecules on amyloid fibrils will serve a good reference to gauge their destabilizing capacity on the amyloid fibrils in the human brain.

Experimental Procedures

Materials. Aβ40 lyophilized powder was purchased from Selleck Chemicals (Houston, TX). Horseradish peroxidase (HRP)-conjugated goat anti-rabbit IgG antibody was obtained from Invitrogen (Carlsbad, CA). 4G8 antibody was obtained from Covance (Dedham, MA). Polyclonal OC and monoclonal 6e10 antibodies were obtained from Millipore (Billerica, MA). Nitrocellulose membranes and ECL Advance chemiluminescence detection kit was obtained from GE Healthcare Life Sciences (Waukesha, WI). Thioflavin T was purchased from Acros Organics (Geel, Belgium). All other chemicals were obtained from Sigma-Aldrich (St. Louis, MO) unless otherwise noted.

Aβ Fibril Formation and Remodeling. Aβ40 fibrils were prepared by dissolving lyophilized Aβ40 peptide powder from Selleck in 100% HFIP at room temperature at a concentration of 1 mM Aβ40. After a 2 hour incubation period at room temperature, the HFIP was evaporated to dryness in a gentle

stream of nitrogen gas. Then, the peptide was diluted to 50 μM Aβ40 in phosphate buffered saline (1X PBS) solution (10 mM NaH_2PO_4 and 150 mM NaCl at pH 7.4) and incubated for 10-13 days at 37°C without stirring. To examine the remodeling effect of brilliant blue G (BBG), methylene blue (MB), and erythrosine B (ER), concentrated stock solutions of each small molecule dissolved in 1X PBS were added to the preformed Aβ40 fibrils. The samples were then incubated for an additional 1 day at 37°C without stirring.

Thioflavin T (ThT) Assay. ThT fluorescence assay was performed as reported previously.[21, 22] Aβ40 fibril formation was monitored by diluting 5 μL of 50 μM Aβ sample solution in 250 μL of 10 μM ThT in black 96-well plates (Fisher Scientific, Pittsburgh, PA). The resulting ThT fluorescence of the Aβ sample was measured at an emission wavelength of 485 nm using an excitation wavelength of 438 nm in a Synergy 4 UV-Vis/fluorescence multi-mode microplate reader (Biotek, VT).

Transmission Electron Microscopy (TEM). Aggregate morphology was assessed using TEM and was performed as reported previously.[21, 22] Aβ samples (10 μL of 50 μM Aβ) were placed on 200 mesh formvar coated/copper grids (Electron Microscopy Sciences, Hatfield, PA), adsorbed for 1 minute, and blotted dry with filter paper. Grids were then negatively stained for 45 seconds with 2% uranyl acetate solution (Electron Microscopy Sciences, Hatfield, PA) in doubly distilled water (ddH_20), blotted dry, and then inspected with a JEOL 1010 Transmission Electron Microscope operated at 60 kV. Aggregate length and width was then quantified where appropriate using Image J software (NIH).

Atomic Force Microscopy (AFM). 10 μL of Aβ samples (diluted to 25 μM Aβ in molecular grade ddH_20) were spotted on freshly cleaved V1 grade muscovite mica (Electron Microscopy Sciences, Hatfield, PA) and allowed to adsorb for 10 minutes. After adsorption, the samples were washed four times with 30 μL molecular grade ddH_20 to remove residual salts, dried with a gentle stream of pure nitrogen gas, and placed in a covered petri dish to dry completely overnight. Dry AFM images were taken using an NT-MDT Solver Pro M system with NSG01 silicon cantilevers (NT-MDT, Santa Clara, CA, guaranteed < 10 nm radius of curvature, 5.1 N/m force constant) in semi-contact mode. Aggregate

length and width was then quantified where appropriate using the Gwyddion SPM analysis software package.[42]

Circular Dichroism (CD) and Numerical Spectra Deconvolution. The secondary structure of Aβ aggregates was evaluated using a Jasco 710 spectropolarimeter (1-mm path length quartz cuvette) at room temperature by diluting 30 μL of 50 μM Aβ sample in 270 μL of ddH_20 (1:10 dilution). The background contribution of the 1X PBS solvent and an appropriate small molecule (BBG, MB, or ER) was then carefully subtracted to obtain the spectra plots displayed. Each background-subtracted sample spectra is the average of at least 10 readings. The background-subtracted sample spectra was then deconvoluted to obtain numerical estimations of secondary structure content using the DichroWeb online circular dichroism analysis software server,[43] employing the CONTINLL analysis program[44, 45] along with 'Set #6'[46, 47] or the SP175[48] reference sets in DichroWeb.

Antibody Dot-Blot Assay. Dot-blot assays were performed as reported previously.[21, 22] 2 μL of 50 μM Aβ samples were loaded on nitrocellulose membranes at the desired time points during fibril destabilization, allowed to air dry, and then were stored at 4°C until immunostaining. For immunostaining, nitrocellulose membranes were first blocked for 1 hour in 5% skim milk dissolved in Tris-buffered saline solution with 0.1% Tween 20 (Bio-Rad, Hercules, CA) (1X TBS-T – 0.05 M Tris base, 0.15 M NaCl, pH 7.44). Membranes were then exposed to three, 5 minute washes with 1X TBS-T. Next, the membranes were incubated for 1 hour with OC (1:14,000 dilution), 6E10 (1:14,000 dilution), or 4G8 (1:7,000 dilution) primary antibody diluted to the specified factor in 0.5% milk 1X TBS-T solution. After the incubation, membranes were then again exposed to three, 5 minute washes with 1X TBS-T. The dot blot intensity of the membrane immuno-stained with 4G8 antibody (already has horseradish peroxidase conjugated) was visualized by exposing the membrane to the ECL substrate (ECL Advance Detection Kit - GE Healthcare) and then imaged in a BioSpectrum imaging system (UVP, Upland, CA). The membranes immunostained with OC and 6E10 antibodies were incubated for 1

hour with HRP-conjugated goat-anti-rabbit IgG secondary antibody at a 1:10,000 dilution in 0.5% milk 1X TBS-T and then visualized using the ECL substrate as described for the 4G8 membrane.

Results and Discussion

BBG Fragments Preformed Aβ Fibrils. Aβ fibrils were prepared by incubating Aβ40 monomers for 10 to 13 days. Thioflavin T (ThT) fluorescence, transmission electron microscopy (TEM), and circular dichroism (CD) assays were employed to verify the formation Aβ fibrils. ThT binding and its resulting fluorescence is widely used to monitor fibril formation.[5] The initiation of fibril assembly is characterized by a sharp increase in ThT fluorescence while mature fibrils are predominantly present when the emission signal reaches a maximum and plateaus. Consequently, Aβ fibril assembly as measured by ThT fluorescence can be modeled by sigmoidal regression. The ThT fluorescence curve in Figure S1 exhibits this behavior. Fibril formation commences on day 5 and ThT fluorescence reaches a maximum by day 10 (Figure S1). Furthermore, from day 9 to day 10, there is no significant increase in ThT fluorescence. Next, TEM was utilized to visually verify the presence of fibrils (Figure 2A; Panel Aβ only and Figure S2 Panel Aβ only for wider frame). Consequently, both ThT fluorescence and TEM results verify that fibrils are present. Next, CD was employed to characterize the secondary structure of the fibrils. The CD spectrum of the Aβ fibrils exhibited the typical features of β-sheet structures (Figure 2B) supporting the fibrillar structure formation.[5]

Next, we investigated whether BBG can destabilize preformed fibrils and generate different forms of aggregates using transmission electron microscopy (TEM), atomic force microscopy (AFM), circular dichroism (CD), and dot-blot assays with Aβ-specific antibodies. Although measuring ThT fluorescence intensity has also been used to monitor a loss of Aβ fibrils, we could not employ this method in our studies due to the reported spectral interference of small molecules including curcumin, BBG, and ER on ThT fluorescence measurement.[5, 21, 22, 49] The preformed Aβ fibrils were then incubated in the absence or presence of BBG for 1 day. First, both the Aβ fibrils and the BBG-treated Aβ fibrils were subjected to negative-stain TEM analysis. The Aβ fibrils exhibited the typical morphological

features of amyloid fibrils. (Figure 2A; Panel Aβ only and Figure S2; Panel Aβ only for wider frame). The length of the Aβ fibril population was measured and found to have an average length of 1,026 ± 621 nm. The population of the fibrils with a length greater than 1,100 nm is 35% (Table 1A). In contrast, BBG treatment generated much shorter aggregates of average length 133 ± 65 nm (Figure 2A; Panel BBG and Figure S2: Panel BBG for wider frame; Table 1A). Although only 6% of the untreated Aβ fibrils have a length less than 300 nm, 97% of the BBG-treated Aβ aggregates have a length less than 300 nm (Table 1A), indicating that the BBG-treated Aβ aggregates were strikingly shorter than the untreated Aβ fibrils. Next, we investigated the morphological trends of the remodeled fibrils observed using AFM. As was the case with the TEM results, most of the untreated Aβ fibrils are intermingled (Figure 2B; Panel Aβ only), while treatment with 10X BBG resulted in much shorter, dispersed aggregates (Figure 2B: Panel BBG). The lengths and widths of the two Aβ samples were measured using the AFM image analysis software Gwyddion[42] (Table S1A and S1B in the Supporting Information). When we first began the AFM analysis of our samples, we expected to be able to directly compare the lengths and widths found with AFM to our TEM results. However, since the intrinsic resolution limit of AFM set by cantilever tip radius affects the absolute values of both lateral and height measurements[50-52] and the detection limit of AFM is smaller than that of TEM,[53, 54] a direct comparison between TEM and AFM values was not possible. Therefore, we focused on comparing the length and width distribution trends between samples obtained using the two different microscopic assays. The average length of the 10X BBG-treated fibrils measured using AFM was 96 ± 40 nm, while the average length of the untreated Aβ fibrils was much longer at 329 ± 161 nm, consistent with the remodeling trend observed in the TEM images. In fact, 89% of the BBG-treated sample had a length less than 150 nm, while only 17% of the amyloid fibril sample had a length less than 150 nm (Table S1A). A decrease in the average lengths of both the untreated and the BBG-treated Aβ fibrils in AFM compared to TEM is likely due to the lower detection limit of AFM than that of TEM. In the TEM results, the percentages of the Aβ aggregates of a length less than 200 nm are 2% and 88% for the untreated and the BBG-treated Aβ fibrils, respectively (Table 1A). However, in AFM results, these values are 30% and 98% (Table S1A),

indicating that small Aβ aggregates were better detected by AFM than TEM resulting in the decrease in the average length in AFM compared to TEM. Despite the differences in absolute average lengths, both the TEM and AFM results strongly support the idea that the BBG-treatment substantially reduces the average length of Aβ fibrils. Therefore, the BBG-treated Aβ aggregate could be protofibrils or fibril fragments.

In order to determine whether the BBG-treated aggregates are protofibrils or fibril fragments, their thicknesses/widths were measured and compared to those of untreated Aβ fibrils. According to the Aβ fibril structural model proposed by Schmidt et. al through cryo-EM and mass-per-length analysis of Aβ40 fibrils and protofibrils,[55] the thicknesses of the individual Aβ fibril and protofibril are around 20 nm and 12 nm, respectively. Despite concern over the intrinsic resolution of the technique, negative-stain TEM has been used numerous times in the literature by different research groups to provide numerical estimation of the length or width of aggregates less than 30 nm.[5, 56-58] More specifically, Fandrich, et al. employed TEM to measure the widths of Aβ40 fibrils and found the average width to be 20.6 ± 2.8 nm,[59] which is in good agreement with the cryo-EM findings.[55] The untreated Aβ fibrils in this study exhibited an average width of 19 ± 4 nm upon examination of the magnified TEM image (Figure 2A; Panel Aβ only_M), with 98% of the fibrils measured having a width greater than 12 nm (Table 1B). Upon examination of the magnified TEM image, thickness of the BBG-treated Aβ aggregates seems similar to that of the untreated Aβ fibrils (Figure 2A; Panel BBG_M). The average width of the BBG-treated Aβ aggregates is 26 ± 7 nm (Table 1B). In particular, none of the aggregates measured have a width of 12 nm or less, clearly indicating that the BBG-treated Aβ aggregates are not protofibrils. Considering that the average width of the BBG-treated Aβ aggregates is comparable to that of the untreated Aβ fibrils, the BBG-treated Aβ aggregates are considered shorter Aβ fibrils compared to the untreated Aβ fibrils. The AFM results also show similar trends in the width of the Aβ aggregates (Table S1B). The average width of the BBG-treated sample was 58 ± 14 nm, and the untreated Aβ fibril sample had an average width of 73 ± 23 nm. In comparing the width distributions of these two samples measured using AFM, it was found that 86% of the BBG-treated sample's aggregate widths fall within

one standard deviation of the Aβ fibril average width, indicating that these samples possess similar widths and confirming the trend found in the TEM analysis. An increase in the average width of the Aβ aggregates obtained using AFM assay compared to those of TEM assay can be attributed to the intrinsic resolution limit set by cantilever tip radius leading to over-estimation (convolution) of nanostructure widths.[50, 51] Because BBG-treatment resulted in shorter aggregates but of similar thickness as Aβ fibrils, we hypothesized that the BBG-induced Aβ aggregates are likely fragmented fibrils but not protofibrils.

In order to confirm this hypothesis, we also performed CD analysis. CD analysis is widely used to analyze secondary structure content of proteins.[5, 60-63] The CD spectra of both the Aβ fibrils and the BBG-treated Aβ fibrils are shown in Figure 2C along with that of Aβ monomers for comparison. In the CD spectrum of Aβ monomers, neither α-helix nor β-sheet structural features were observed, strongly suggesting that Aβ monomers have disordered structure (Figure 2C). However, the CD spectrum of the Aβ fibrils exhibited the typical features of β-sheet-rich structure,[5] including a minimum at 217 nm (Figure 2C). The BBG-treated Aβ fibrils maintained the typical features of β-sheet structure. The minimum ellipticity value of the BBG-treated Aβ fibrils was observed at 217 nm. The ellipticity of the BBG-treated Aβ fibrils was positive below 200 nm. In order to quantitatively investigate secondary structural changes caused by BBG treatment, we used the web-based server, DichroWeb,[43] and calculated the secondary structure contents from the CD spectra using the CONTIN analysis program[44, 45] and SP175 reference protein set.[43, 48] The α-helix, β-sheet, β-turn, and disordered structure content of the Aβ fibrils are 12.2%, 36.4%, 12.1%, and 39.3% (Table 2), respectively, which is consistent with the Aβ fibril structural information that the N-terminus 17 residues (residues 1 – 17) are usually disordered and the 6 residues (residues 23-28) in the middle of Aβ sequence form β-turn structure.[57] Upon one day incubation of the Aβ fibrils with BBG, the secondary structural content was only slightly changed, with the β-sheet content increasing by 8% but the disordered structure content decreasing by around 7%. The β-sheet content of the BBG-treated Aβ fibrils is comparable to that of the Aβ fibril control, suggesting that the BBG-treated Aβ fibrils also have fibrillar structures similar to the Aβ fibril control. Considering that the BBG-treated Aβ fibrils have fibrillar structures in the TEM image, these results support the idea

that the BBG-treated Aβ aggregates are shorter Aβ fibrils than the untreated Aβ fibril control, likely Aβ fibril fragments.

Dot-blot assays of the Aβ samples were also performed using three Aβ-specific antibodies (OC, 4G8, and 6E10). Recently, dot-blotting with Aβ-specific antibodies has been widely used to detect Aβ aggregates with different conformations.[5, 64-70] OC is a polyclonal antibody that recognizes fibrillar oligomers, protofibrils and fibrils but not monomer, prefibrillar oligomers, and disordered aggregates.[66, 68] 4G8 is an Aβ sequence-specific monoclonal antibody,[71-74] which binds to amino acids 17 to 24 of Aβ. Lastly, 6E10 is a monoclonal antibody that recognizes residues 1-16 of Aβ.[66, 75] Although both 4G8 and 6E10 were originally used to ensure the conservation of Aβ moieties, recent findings demonstrated that immuno-reactivities of these two antibodies can be affected by Aβ conformational changes and small-molecule binding to their epitopes.[21, 22, 75] In order to distinguish the immuno-reactivity changes caused by the small molecules binding to antibody epitopes (fast processes) from those made by Aβ conformation changes (slow processes), we incubated the Aβ fibrils with the small molecules for a very short time (less than 5 min) and for a longer time (one day). Incubation of the Aβ fibrils with 1x BBG (molar concentration equal to that of Aβ peptide) did not alter the immuno-reactivities of Aβ fibrils for all three antibodies (OC, 6E10, and 4G8), strongly indicating that there is no change in the content of fibrillar structure (Figure 3). The 6E10 and 4G8 immuno-reactivities of the BBG-treated fibril samples at both 5 minutes and 1 day were maintained when compared to the fibril sample, indicating that BBG did not significantly bind to the 1-16 and 17-24 residues of Aβ. It is noteworthy that 10x BBG (10 times the molar concentration of Aβ peptide) resulted in a significant reduction of the OC-reactivity after 1-day incubation (Figure 3; Panel 1-day incubation). However, such a reduction in the OC-reactivity of the 10x BBG-treated Aβ fibrils can be explained by BBG binding to the OC epitope rather than a loss of fibrillar structure. The short incubation of Aβ fibrils with 10x BBG is not long enough to cause Aβ conformational changes resulting in a significant reduction in the OC-reactivity (Figure 3; Panel < 5 min), indicating that BBG binds to the epitope thus restricting the access of the OC antibody. It was

also reported that BBG binds to Aβ peptide in multiple sites.[21] Therefore, we speculate that direct binding of BBG to Aβ fibrils leads to Aβ fibril fragmentation, though more studies are required to identify Aβ residues or local structures of Aβ fibrils interacting with BBG.

MB Converts Preformed Aβ fibrils into Amorphous Aggregates. Next, Aβ fibrils were treated with 1x or 10x MB for one day. The TEM and AFM images of the MB-treated Aβ fibrils showed that no structural features of fibrils were observed, and neither the size nor the shape of the MB-treated Aβ aggregates were homogenous (Figure 4A), indicating the possibility of structural changes from fibrils to amorphous aggregates. The CD spectrum of the MB-treated Aβ fibrils showed three changes from that of Aβ fibrils - a shift in the wavelength of a minimum ellipticity, negative ellipticity below 200 nm, and an upward shift of ellipticity above 200 nm toward zero (Figure 4B). Furthermore, the CD spectrum of the MB-treated Aβ fibrils shifted toward that of the Aβ monomers (Figure 4B). Because Aβ monomers have been shown to possess predominantly disordered/random-coil secondary structure[5, 60] and low ellipticity above 210 nm and negative banding at 195 nm are general characteristics of disordered proteins,[76] the changes observed with MB-treated fibrils strongly indicate a substantial loss of the β-sheet content but an increase in the disordered structural content. Similar to the BBG-treated Aβ fibrils, the CD spectrum of the MB-treated Aβ fibrils was used to estimate the secondary structure content numerically using DichroWeb. Because the SP175 reference set contains the greatest range of protein structures/conformations among the total eight reference sets explicitly described in DichroWeb, our first choice was to employ this reference set for the CD analysis with all three small molecules (BBG, MB, and ER). However, when we used the SP175 reference protein set to analyze the MB-treated fibril CD spectrum, no significant change in the secondary structure content was observed despite the obvious changes in the spectrum described previously (Table S2 in the Supporting Information). After searching through the literature for a possible explanation to this disparity, we found that the accuracy of the secondary structure content deconvolution estimation greatly relies on the choice of a reference protein

set containing proteins with similar structure to the one being studied.[43, 47] Since many of the intrinsically disordered amyloidogenic proteins do not fold into only one stable conformation that can be used to construct a reference set, finding an appropriate reference set for intrinsically disordered Aβ is particularly challenging. To our knowledge, there are no existing reference sets containing intrinsically disordered monomeric peptides/proteins, such as Aβ monomer. After thoroughly examining the SP175 reference protein set,[48] we found that α-helix-, β-sheet, and β-turn -rich reference proteins are well represented in the SP175 reference set, allowing successful estimation of the secondary structure contents of numerous folded proteins. However, we also found that the SP175 set includes only 1-2 disordered reference proteins among a total of 72 reference proteins. Since the proteins used to construct the SP175 reference set were prepared by folding recombinant proteins produced from bacteria, denatured or unfolded proteins were rarely included. Such a relatively low frequency of the disordered reference proteins is most likely attributed to the underestimated disordered structure content. In fact, the developers of the SP175 reference set also acknowledged that the validity of the reference set is limited to α-helical and β-rich proteins, not disordered proteins.[48] This further underlines the importance of performing an in-depth review of the reference set being used before beginning the analysis.

In order to address the issue of finding an appropriate reference set for the spectrum of the MB-treated Aβ fibrils, different reference protein sets contained within the DichroWeb server were evaluated. Among the reference protein sets embedded in DichroWeb, Set No. 6 has the highest frequency of disordered reference proteins (11 out of 42 total reference proteins). Therefore, the secondary structure contents of both the Aβ fibrils and the MB-treated Aβ fibrils were re-evaluated using the Set No. 6 and the estimated values are presented in Table 3. Compared to the Aβ fibrils, the MB-treated Aβ fibrils exhibited a significant reduction in the β-sheet and β-turn content, but a substantial increase in the unordered structure content, which is quite consistent with the observation of the amorphous aggregates in the TEM monograph, AFM scan (Figure 4A), and qualitative visual analysis of the CD spectra. To our knowledge, conversion of Aβ fibrils into disordered-structured

aggregates has not been shown previously through numerical deconvolution analysis of corresponding CD spectra.

The interaction between MB and preformed Aβ40 fibrils was further explored using dot-blotting with 6E10, OC, and 4G8 antibodies. Incubation of Aβ fibrils with either 1x or 10x MB for a very short time (less than 5 min) led to a substantial loss of the OC-reactivity (Figure 3; Panel < 5 min), clearly indicating that MB binds to the OC antibody epitope. Because of this strong binding affinity of MB to the OC antibody epitope, it is difficult to discern whether the weak OC signals observed in the MB-treated fibrils for 1 day (Figure 3, Panel 1 day) can be attributed to the direct MB binding to the OC epitope or the structural changes induced by MB (resulting in loss of the cross-stacked β-sheet epitope). The Aβ fibrils treated with MB for a short time also led to a complete loss of the 6E10 reactivity, indicating that MB binds to the 6E10 antibody epitope (residues 1 – 16 of Aβ). According to the structural model of Aβ fibrils, the N-terminus of Aβ (residues 1 – 16) is involved in the assembly of two protofibrils into one fibril.[55] Therefore, we speculate that MB destabilizes fibrils into amorphous aggregates at least in part via MB binding to a joint region between the two protofibrillar components of an Aβ fibril.

ER Disrupts Preformed Aβ fibrils into Protofibrils. In order to investigate the action of the third small molecule modulator, 1x or 10x ER was incubated with the Aβ fibrils for one day. The TEM image of the ER-treated Aβ fibrils showed many fibrillar structures (Figure 5A and Figure S2; ER panel for wider frame) that seemed to be less tightly bundled/stacked than the untreated fibril sample (Figure 2A-B; Aβ only panels and Figure S2; Aβ only panel). The average length of the ER-treated fibrils measured using TEM was 303 ± 129 nm, less than the average length of the untreated fibrils mentioned previously, but longer than the fibrils treated with 10X BBG (Table 1A). The majority (73%) of the ER-treated aggregates measured had a length between 200 and 500 nm. Next, the morphological fate trends of Aβ fibrils remodeled with ER were investigated using AFM and compared to the TEM findings. Similar to TEM, the AFM scan of the ER-treated Aβ fibrils (Figure 5B) showed many fibrillar

structures, still in close proximity to each other, but less stacked than with the untreated fibril sample (Figure 2B; Aβ only panel). From the AFM scan, the average length of the ER-treated sample was found to be 162 ± 60 nm (Table S1 in Supporting Information). This length data matched the trend seen in the TEM data that the ER-treated fibrils were shorter than the untreated Aβ fibrils, but longer than the BBG-treated sample's aggregate population. As was the case for the untreated- and the BBG-treated Aβ samples, the average length of the ER-treated sample measured by AFM is shorter than that by TEM, likely because AFM detects shorter Aβ aggregates better than TEM. The ER-treated Aβ aggregates that are shorter than the untreated Aβ fibrils could be protofibrils or Aβ fibril fragments.

In order to determine whether the ER-treated aggregates are protofibrils or fibril fragments, their widths were measured and compared to those of untreated Aβ fibrils. From the TEM images (Figure 5A and Figure S2 in the Supporting Information), the average width of the ER-induced aggregates is significantly smaller than that of both the untreated Aβ fibrils and the 10X BBG-treated Aβ fibrils (Table 1B). The average measured width of the ER-treated Aβ fibrils was 10 ± 2 nm, which matches well with the width of individual protofibril according to the Aβ protofibrils and fibrils structural model discussed previously.[55] Furthermore, none of the ER-treated Aβ fibrils measured displayed widths greater than 16 nm, whereas 78% and 99%, respectively, of the untreated Aβ fibrils and the BBG-treated fibrils samples measured contained widths greater than the 16 nm cutoff. It is also noteworthy to mention that co-incubation of Aβ monomer with ER also led to formation of dominant protofibrils with the width of 12 nm.[22] Furthermore, the ER-treated samples did not exhibit the twisted structure, a typical feature of Aβ fibrils in general and also observed in our untreated Aβ fibril samples, in the TEM images (Figure 5A for ER-treated sample and Figure 2A for Aβ only sample). Moreover, the widths of the ER-treated aggregates (35 ± 6 nm) analyzed using AFM were much thinner than the Aβ fibril (73 ± 23 nm) and BBG-treated samples (58 ± 14 nm) (Table S1B in the Supporting Information), reinforcing the trend found in the TEM analysis. In fact, the width distribution data show that only 6% of the ER-treated sample's aggregate population displayed widths within one standard deviation from the 73 nm mean width for the untreated fibril sample. Because of these morphological changes/findings, the ER-treated

Aβ fibrils are most likely protofibrils. As was the case for the untreated Aβ fibrils and the BBG-treated Aβ fibrils, the width of the ER-treated Aβ fibrils determined by AFM is considered over-estimated compared to the width determined of TEM due to the lateral convolution caused by cantilever tip radius.[50, 51]

The CD spectrum of the ER-treated Aβ fibrils clearly shows typical features of β-sheet-rich structure (Figure 5C). The estimates of the secondary structure content of the ER-treated Aβ fibrils are essentially the same as those of Aβ fibrils (Table 2), indicating that the ER-treated Aβ fibrils are β-sheet -rich, and most likely fibrillar structures.

In the dot-blot assays, the short time incubation (less than 5 minutes) of the Aβ fibrils with 1x or 10x ER led to a significant reduction of the OC-reactivity (Figure 3), clearly indicating that ER binds to the OC antibody epitope (as was the case with MB). Further, both 1x and 10x ER led to a complete loss of the 6E10 reactivity indicating that a primary ER binding site on Aβ is located at the 6E10 antibody epitope (Aβ N-terminus), which is consistent with the results reported previously.[22] As mentioned previously in the structural model of Aβ fibrils, the N-terminus of Aβ (residues 1 – 16) is involved in the assembly of two protofibrils into one fibril. Therefore, we conclude that ER separates fibrils in to the ER-induced protofibrils by binding to the N-terminus of the two protofibrillar components of Aβ fibrils, thus destabilizing the fibril complex. Although both MB and ER were shown to bind to the N-terminus of Aβ sequence, they most likely interact with different residues in Aβ. MB has a positive charge, but ER has negative charges. Therefore, we speculate that MB and ER interact with negatively and positively charged residues in the N-terminus of Aβ, respectively, which led to different fates of the destabilized Aβ fibrils.

Conclusions

In this article, we evaluated three biocompatible small molecule Aβ aggregation modulators (BBG, MB, and ER) for their capacities to trigger structural changes of the Aβ fibrils in a physiologically-relevant manner and then characterized the structural features of the restructured Aβ

fibrils and the mechanisms by which the changes occur. Combined with TEM, AFM, and dot-blot assays, conversion of Aβ fibrils into different types of aggregates was quantitatively analyzed through numerical deconvolution analysis of corresponding CD spectra with appropriate choices of reference protein sets. Incubation of the preformed Aβ fibrils with these molecules (BBG, MB, and ER) effectively destabilized the preformed Aβ fibrils but led to three distinct fates. BBG fragmented the Aβ fibrils into shorter fibrils. MB restructured the Aβ fibrils into amorphous aggregates. Finally, ER separated the Aβ fibrils into protofibrils. We found that BBG binds to the OC antibody epitope. Previously, it was shown that BBG binds to Aβ peptide in multiple sites.[21] Therefore, it is likely that direct binding of BBG to Aβ fibrils causes the Aβ fibril fragmentation. We also found that both MB and ER bind to the N-terminus of Aβ, a joining of two protofibrils to form one Aβ fibril. Therefore, we speculate that MB or ER binding to the join two protofibrils is a key step that triggers drastic structural changes of the Aβ fibrils into amorphous aggregates or separate protofibrils, respectively. Our investigation has conclusively established that the preformed Aβ fibrils can be destabilized or remodeled by three small molecules (BBG, MB, and ER). These three biocompatible molecules are promising candidates to remove insoluble amyloid fibrils deposited in the human brain. Our results also successfully illustrate the possibility of controlling changes in biomolecule-based nanostructures using chemical compounds.

Acknowledgment

We thank Dr. Alev Erisir and Anqi Fu at the Psychology Department at the University of Virginia for assistance with TEM assays on Aβ samples. We are grateful to Dr. Jerold Floro, Joseph Kassim, and Jatin Amatya at the Material Science Department at the University of Virginia for assistance with AFM assays. We also thank Dr. Peter Tessier at the Rensselaer Polytechnic Institute for insightful discussion on the aggregation of Aβ with MB. This work was supported by the KSEA Young Investigator Grant to I. K. and a National Science Foundation Graduate Research Fellowship to J. A. I. (DGE-00809128).

Supporting Information Available: Additional data (Figure S1, S2 and Table S1, S2). This material is available free of charge via the Internet at http://pubs.acs.org.

References

1. Hardy, J.; Higgins, G., Alzheimer's Disease: The Amyloid Cascade Hypothesis. *Science* **1992,** 256, 184-185.

2. Li, J.; Uversky, V. N.; Fink, A. L., Effect of familial Parkinson's disease point mutations A30P and A53T on the structural properties, aggregation, and fibrillation of human alpha-synuclein. *Biochemistry* **2001,** 40, (38), 11604-11613.

3. Li, J.; Zhu, M.; Rajamani, S.; Uversky, V. N.; Fink, A. L., Rifampicin Inhibits α-Synuclein Fibrillation and Disaggregates Fibrils. *Chem. Biol. (Cambridge, MA, U. S.)* **2004,** 11, (11), 1513-1521.

4. Spillantini, M. G.; Crowther, R. A.; Jakes, R.; Cairns, N. J.; Lantos, P. L.; Goedert, M., Filamentous alpha-synuclein inclusions link multiple system atrophy with Parkinson's disease and dementia with Lewy bodies. *Neurosci. Lett.* **1998,** 251, (3), 205-208.

5. Gregoire, S.; Irwin, J.; Kwon, I., Techniques for monitoring protein misfolding and aggregation in vitro and in living cells. *Korean J. Chem. Eng.* **2012,** 29, (6), 693-702.

6. Jahn, T. R.; Radford, S. E., The Yin and Yang of protein folding. *FEBS J.* **2005,** 272, (23), 5962-5970.

7. Jones, O. G.; Mezzenga, R., Inhibiting, promoting, and preserving stability of functional protein fibrils. *Soft Matter* **2012,** 8, (4), 876-895.

8. Chatani, E.; Lee, Y.-H.; Yagi, H.; Yoshimura, Y.; Naiki, H.; Goto, Y., Ultrasonication-dependent production and breakdown lead to minimum-sized amyloid fibrils. *Proc. Natl. Acad. Sci. U. S. A.* **2009,** 106, (27), 11119-11124.

9. Arora, A.; Ha, C.; Park, C. B., Insulin amyloid fibrillation at above 100°C: New insights into protein folding under extreme temperatures. *Protein Sci.* **2004,** 13, (9), 2429-2436.

10. Dubois, J.; Ismail; Chan; Ali, K., Fourier Transform Infrared Spectroscopic Investigation of Temperature- and Pressure-Induced Disaggregation of Amyloid A. *Scand. J. Immunol.* **1999,** 49, (4), 376-380.

11. Adamcik, J.; Mezzenga, R., Adjustable twisting periodic pitch of amyloid fibrils. *Soft Matter* **2011,** 7, (11), 5437-5443.

12. Narimoto, T.; Sakurai, K.; Okamoto, A.; Chatani, E.; Hoshino, M.; Hasegawa, K.; Naiki, H.; Goto, Y., Conformational stability of amyloid fibrils of β2-microglobulin probed by guanidine-hydrochloride-induced unfolding. *FEBS Lett.* **2004,** 576, (3), 313-319.

13. Hirota-Nakaoka, N.; Hasegawa, K.; Naiki, H.; Goto, Y., Dissolution of β2-Microglobulin Amyloid Fibrils by Dimethylsulfoxide. *J. Biochem.* **2003,** 134, (1), 159-164.

14. Jordens, S.; Adamcik, J.; Amar-Yuli, I.; Mezzenga, R., Disassembly and Reassembly of Amyloid Fibrils in Water−Ethanol Mixtures. *Biomacromolecules* **2010,** 12, (1), 187-193.

15. Li, J.; Zhu, M.; Manning-Bog, A. B.; Di Monte, D. A.; Fink, A. L., Dopamine and L-dopa disaggregate amyloid fibrils: implications for Parkinson's and Alzheimer's disease. *FASEB J.* **2004,** 18, (9), 962-964.

16. Benilova, I.; Karran, E.; De Strooper, B., The toxic A[beta] oligomer and Alzheimer's disease: an emperor in need of clothes. *Nat. Neurosci.* **2012,** 15, (3), 349-357.

17. Ruhs, P. A.; Adamcik, J.; Bolisetty, S.; Sanchez-Ferrer, A.; Mezzenga, R., A supramolecular bottle-brush approach to disassemble amyloid fibrils. *Soft Matter* **2011,** 7, (7), 3571-3579.

18. Park, J.-W.; Lee, I.-H.; Hahn, J.-S.; Kim, J.; Chung, K. C.; Paik, S. R., Disintegration of amyloid fibrils of α-synuclein by dequalinium. *Biochim. Biophys. Acta, Gen. Subj.* **2008,** 1780, (10), 1156-1161.

19. Giorgetti, S.; Raimondi, S.; Pagano, K.; Relini, A.; Bucciantini, M.; Corazza, A.; Fogolari, F.; Codutti, L.; Salmona, M.; Mangione, P.; Colombo, L.; De Luigi, A.; Porcari, R.; Gliozzi, A.; Stefani, M.; Esposito, G.; Bellotti, V.; Stoppini, M., Effect of Tetracyclines on the Dynamics of Formation and Destructuration of β2-Microglobulin Amyloid Fibrils. *J. Biol. Chem.* **2011,** 286, (3), 2121-2131.

20. Bieschke, J.; Russ, J.; Friedrich, R. P.; Ehrnhoefer, D. E.; Wobst, H.; Neugebauer, K.; Wanker, E. E., EGCG remodels mature alpha-synuclein and amyloid-beta fibrils and reduces cellular toxicity. *Proc. Natl. Acad. Sci. U. S. A.* **2010,** 107, (17), 7710-7715.

21. Wong, H. E.; Qi, W.; Choi, H.-M.; Fernandez, E. J.; Kwon, I., A Safe, Blood-Brain Barrier Permeable Triphenylmethane Dye Inhibits Amyloid-β Neurotoxicity by Generating Nontoxic Aggregates. *ACS Chem. Neurosci.* **2011,** 2, (11), 645-657.

22. Wong, H. E.; Kwon, I., Xanthene Food Dye, as a Modulator of Alzheimer's Disease Amyloid-beta Peptide Aggregation and the Associated Impaired Neuronal Cell Function. *PLoS ONE* **2011,** 6, (10), e25752.

23. Ladiwala, A. R. A.; Dordick, J. S.; Tessier, P. M., Aromatic Small Molecules Remodel Toxic Soluble Oligomers of Amyloid-beta through Three Independent Pathways. *J. Biol. Chem.* **2011,** 286, (5), 3209-3218.

24. Necula, M.; Breydo, L.; Milton, S.; Kayed, R.; van der Veer, W. E.; Tone, P.; Glabe, C. G., Methylene blue inhibits amyloid Abeta oligomerization by promoting fibrillization. *Biochemistry* **2007,** 46, (30), 8850-60.

25. Callaway, N. L.; Riha, P. D.; Wrubel, K. M.; McCollum, D.; Gonzalez-Lima, F., Methylene blue restores spatial memory retention impaired by an inhibitor of cytochrome oxidase in rats. *Neurosci. Lett.* **2002,** 332, (2), 83-86.

26. Korth, C.; May, B. C.; Cohen, F. E.; Prusiner, S. B., Acridine and phenothiazine derivatives as pharmacotherapeutics for prion disease. *Proc. Natl. Acad. Sci. U. S. A.* **2001,** 98, (17), 9836-41.

27. Borzelleca, J. F.; Hallagan, J. B., Multigeneration study of FD & C Red No. 3 (erythrosine) in Sprague-Dawley rats. *Food Chem. Toxicol.* **1990,** 28, (12), 813-9.

28. Levitan, H.; Ziylan, Z.; Smith, Q. R.; Takasato, Y.; Rapoport, S. I., Brain uptake of a food dye, erythrosin B, prevented by plasma protein binding. *Brain Res.* **1984,** 322, (1), 131-4.

29. Shin, H.-J.; Lee, E.-K.; Lee, J.-H.; Lee, D.; Chang, C.-S.; Kim, Y.-S.; Paik, S. R., Eosin interaction of α-synuclein leading to protein self-oligomerization. *Biochim. Biophys. Acta, Protein Struct. Mol. Enzymol.* **2000,** 1481, (1), 139-146.

30. Gardner, D. F.; Utiger, R. D.; Schwartz, S. L.; Witorsch, P.; Meyers, B.; Braverman, L. E.; Witorsch, R. J., Effects of oral erythrosine (2′ ,4′ ,5′ ,7′ -tetraiodofluorescein) on thyroid function in normal men. *Toxicol. Appl. Pharmacol.* **1987,** 91, (3), 299-304.

31. Hirohashi, T.; Terasaki, T.; Shigetoshi, M.; Sugiyama, Y., In Vivo and In Vitro Evidence for Nonrestricted Transport of 2′ ,7′ -Bis(2-Carboxyethyl)-5(6)-Carboxyfluorescein Tetraacetoxymethyl Ester at the Blood-Brain Barrier. *J. Pharmacol. Exp. Ther.* **1997,** 280, (2), 813-819.

32. Remy, M.; Thaler, S.; Schumann, R. G.; May, C. a.; Fiedorowicz, M.; Schuettauf, F.; Grüterich, M.; Priglinger, S. G.; Nentwich, M. M.; Kampik, a.; Haritoglou, C., An in vivo evaluation of Brilliant Blue G in animals and humans. *Br. J. Ophthalmol.* **2008,** 92, (8), 1142-7.

33. Peng, W.; Cotrina, M. L.; Han, X.; Yu, H.; Bekar, L.; Blum, L.; Takano, T.; Tian, G.-F.; Goldman, S. A.; Nedergaard, M., Systemic administration of an antagonist of the ATP-sensitive receptor P2X7 improves recovery after spinal cord injury. *Proc. Natl. Acad. Sci. U. S. A.* **2009,** 106, (30), 12489-12493.

34. Borzelleca Joseph, F.; Hallagan John, B., Safety and Regulatory Status of Food, Drug, and Cosmetic Color Additives. In *Food Safety Assessment*, American Chemical Society: 1992; Vol. 484, pp 377-390.

35. Borzelleca, J. F.; Depukat, K.; Hallagan, J. B., Lifetime toxicity/carcinogenicity studies of FD & C blue No. 1 (Brilliant blue FCF) in rats and mice. *Food Chem. Toxicol.* **1990,** 28, (4), 221-234.

36. Ryu, J. K.; McLarnon, J. G., Block of purinergic P2X7 receptor is neuroprotective in an animal model of Alzheimer's disease. *NeuroReport* **2008,** 19, (17), 1715-1719.

37. Matute, C.; Torre, I.; Pérez-Cerdá, F.; Pérez-Samartín, A.; Alberdi, E.; Etxebarria, E.; Arranz, A. M.; Ravid, R.; Rodríguez-Antigüedad, A.; Sánchez-Gómez, M.; Domercq, M., P2X7 Receptor Blockade Prevents ATP Excitotoxicity in Oligodendrocytes and Ameliorates Experimental Autoimmune Encephalomyelitis. *J. Neurosci.* **2007,** 27, (35), 9525-9533.

38. Simmons, R.; Thevarajah, S.; Brennan, M.; Christos, P.; Osborne, M., Methylene Blue Dye as an Alternative to Isosulfan Blue Dye for Sentinel Lymph Node Localization. *Ann. Surg. Onc.* **2003,** 10, (3), 242-247.

39. Thevarajah, S.; Huston, T. L.; Simmons, R. M., A comparison of the adverse reactions associated with isosulfan blue versus methylene blue dye in sentinel lymph node biopsy for breast cancer. *Am. J. Surg.* **2005,** 189, (2), 236-239.

40. Zoungrana, A.; Coulibaly, B.; Sié, A.; Walter-Sack, I.; Mockenhaupt, F. P.; Kouyaté, B.; Schirmer, R. H.; Klose, C.; Mansmann, U.; Meissner, P.; Müller, O., Safety and Efficacy of Methylene Blue Combined with Artesunate or Amodiaquine for Uncomplicated Falciparum Malaria: A Randomized Controlled Trial from Burkina Faso. *PLoS ONE* **2008,** 3, (2), e1630.

41. Medina, D. X.; Caccamo, A.; Oddo, S., Methylene Blue Reduces Aβ Levels and Rescues Early Cognitive Deficit by Increasing Proteasome Activity. *Brain Pathol.* **2011,** 21, (2), 140-149.

42. http://gwyddion.net/

43. Whitmore, L.; Wallace, B. A., Protein secondary structure analyses from circular dichroism spectroscopy: Methods and reference databases. *Biopolymers* **2008,** 89, (5), 392-400.

44. Provencher, S. W.; Gloeckner, J., Estimation of globular protein secondary structure from circular dichroism. *Biochemistry* **1981,** 20, (1), 33-37.

45. Vanstokkum, I., Estimation of protein secondary structure and error analysis from circular dichroism spectra. *Anal. Biochem.* **1990,** 191, (1), 110-118.

46. Sreerama, N.; Woody, R. W., Estimation of Protein Secondary Structure from Circular Dichroism Spectra: Comparison of CONTIN, SELCON, and CDSSTR Methods with an Expanded Reference Set. *Anal. Biochem.* **2000,** 287, (2), 252-260.

47. Sreerama, N.; Venyaminov, S. Y.; Woody, R. W., Estimation of Protein Secondary Structure from Circular Dichroism Spectra: Inclusion of Denatured Proteins with Native Proteins in the Analysis. *Anal. Biochem.* **2000,** 287, (2), 243-251.

48. Lees, J. G.; Miles, A. J.; Wien, F.; Wallace, B. A., A reference database for circular dichroism spectroscopy covering fold and secondary structure space. *Bioinformatics* **2006,** 22, (16), 1955-1962.

49. Hudson, S. a.; Ecroyd, H.; Kee, T. W.; Carver, J. a., The thioflavin T fluorescence assay for amyloid fibril detection can be biased by the presence of exogenous compounds. *FEBS J.* **2009,** 276, (20), 5960-72.

50. Del Mercato, L. L.; Maruccio, G.; Pompa, P. P.; Bochicchio, B.; Tamburro, A. M.; Cingolani, R.; Rinaldi, R., Amyloid-like Fibrils in Elastin-Related Polypeptides: Structural Characterization and Elastic Properties. *Biomacromolecules* **2008,** 9, (3), 796-803.

51. Santos, S.; Barcons, V.; Christenson, H. K.; Font, J.; Thomson, N. H., The Intrinsic Resolution Limit in the Atomic Force Microscope: Implications for Heights of Nano-Scale Features. *PLoS ONE* **2011,** 6, (8), e23821.

52. Pires, R. H.; Saraiva, M. J.; Damas, A. M.; Kellermayer, M. S. Z., Structure and assembly–disassembly properties of wild-type transthyretin amyloid protofibrils observed with atomic force microscopy. *J. Mol. Recognit.* **2011,** 24, (3), 467-476.

53. Stine, W. B.; Dahlgren, K. N.; Krafft, G. a.; LaDu, M. J., In vitro characterization of conditions for amyloid-beta peptide oligomerization and fibrillogenesis. *J. Biol. Chem.* **2003,** 278, (13), 11612-22.

54. Langkilde, A. E.; Vestergaard, B., Methods for structural characterization of prefibrillar intermediates and amyloid fibrils. *FEBS Lett.* **2009,** 583, (16), 2600-9.

55. Schmidt, M.; Sachse, C.; Richter, W.; Xu, C.; Fändrich, M.; Grigorieff, N., Comparison of Alzheimer Aβ(1–40) and Aβ(1–42) amyloid fibrils reveals similar protofilament structures. *Proc. Natl. Acad. Sci. U. S. A.* **2009,** 106, (47), 19813-19818.

56. Woods, L. a.; Platt, G. W.; Hellewell, A. L.; Hewitt, E. W.; Homans, S. W.; Ashcroft, A. E.; Radford, S. E., Ligand binding to distinct states diverts aggregation of an amyloid-forming protein. *Nat. Chem. Biol.* **2011,** 7, (10), 730-9.

57. Ahmed, M.; Davis, J.; Aucoin, D.; Sato, T.; Ahuja, S.; Aimoto, S.; Elliott, J. I.; Van Nostrand, W. E.; Smith, S. O., Structural conversion of neurotoxic amyloid-beta(1-42) oligomers to fibrils. *Nat. Struct. Mol. Biol.* **2010,** 17, (5), 561-567.

58. Chimon, S.; Shaibat, M. a.; Jones, C. R.; Calero, D. C.; Aizezi, B.; Ishii, Y., Evidence of fibril-like beta-sheet structures in a neurotoxic amyloid intermediate of Alzheimer's beta-amyloid. *Nat. Struct. Mol. Biol.* **2007,** 14, (12), 1157-1164.

59. Klement, K.; Wieligmann, K.; Meinhardt, J.; Hortschansky, P.; Richter, W.; Fändrich, M., Effect of Different Salt Ions on the Propensity of Aggregation and on the Structure of Alzheimer's Aβ(1-40) Amyloid Fibrils. *J. Mol. Biol.* **2007,** 373, (5), 1321-1333.

60. Bartolini, M.; Bertucci, C.; Bolognesi, M. L.; Cavalli, A.; Melchiorre, C.; Andrisano, V., Insight into the kinetic of amyloid beta (1-42) peptide self-aggregation: elucidation of inhibitors' mechanism of action. *ChemBioChem* **2007,** 8, (17), 2152-61.

61. Bitan, G.; Kirkitadze, M. D.; Lomakin, A.; Vollers, S. S.; Benedek, G. B.; Teplow, D. B., Amyloid Beta-protein assembly: Aβ40 and Aβ42 oligomerize through distinct pathways. *Proc. Natl. Acad. Sci. U. S. A.* **2003,** 100, (1), 330-335.

62. Harada, T.; Kuroda, R., CD measurements of β-amyloid (1-40) and (1-42) in the condensed phase. *Biopolymers* **2011,** 95, (2), 127-34.

63. Soto, C.; Castaño, E. M.; Frangione, B.; Inestrosa, N. C., The -Helical to -Strand Transition in the Amino-terminal Fragment of the Amyloid -Peptide Modulates Amyloid Formation. *J. Biol. Chem.* **1995,** 270, (7), 3063-3067.

64. Chen, Y.-R.; Glabe, C. G., Distinct Early Folding and Aggregation Properties of Alzheimer Amyloid-β Peptides Aβ40 and Aβ42. *J. Biol. Chem.* **2006,** 281, (34), 24414-24422.

65. Kayed, R.; Head, E.; Thompson, J. L.; McIntire, T. M.; Milton, S. C.; Cotman, C. W.; Glabe, C. G., Common structure of soluble amyloid oligomers implies common mechanism of pathogenesis. *Science* **2003,** 300, (5618), 486-9.

66. Kayed, R.; Head, E.; Sarsoza, F.; Saing, T.; Cotman, C. W.; Necula, M.; Margol, L.; Wu, J.; Breydo, L.; Thompson, J. L.; Rasool, S.; Gurlo, T.; Butler, P.; Glabe, C. G., Fibril specific, conformation dependent antibodies recognize a generic epitope common to amyloid fibrils and fibrillar oligomers that is absent in prefibrillar oligomers. *Mol. Neurodegener.* **2007,** 2, 18.

67. Wu, J. W.; Breydo, L.; Isas, J. M.; Lee, J.; Kuznetsov, Y. G.; Langen, R.; Glabe, C., Fibrillar oligomers nucleate the oligomerization of monomeric amyloid beta but do not seed fibril formation. *J. Biol. Chem.* **2010,** 285, (9), 6071-9.

68. Ladiwala, A. R. A.; Lin, J. C.; Bale, S. S.; Marcelino-Cruz, A. M.; Bhattacharya, M.; Dordick, J. S.; Tessier, P. M., Resveratrol selectively remodels soluble oligomers and fibrils of amyloid Abeta into off-pathway conformers. *J. Biol. Chem.* **2010,** 285, (31), 24228-24237.

69. Hu, Y.; Su, B.; Kim, C.-S.; Hernandez, M.; Rostagno, A.; Ghiso, J.; Kim, J. R., A strategy for designing a peptide probe for detection of β-amyloid oligomers. *ChemBioChem* **2010,** 11, (17), 2409-18.

70. Williams, A. D.; Sega, M.; Chen, M.; Kheterpal, I.; Geva, M.; Berthelier, V.; Kaleta, D. T.; Cook, K. D.; Wetzel, R., Structural properties of Aβ protofibrils stabilized by a small molecule. *Proc. Natl. Acad. Sci. U. S. A.* **2005,** 102, (20), 7115-7120.

71. Iijima, K.; Liu, H. P.; Chiang, A. S.; Hearn, S. A.; Konsolaki, M.; Zhong, Y., Dissecting the pathological effects of human A beta 40 and A beta 42 in Drosophila: A potential model for Alzheimer's disease. *Proc. Natl. Acad. Sci. U. S. A.* **2004,** 101, (17), 6623-6628.

72. Kimura, N.; Yanagisawa, K.; Terao, K.; Ono, F.; Sakakibara, I.; Ishii, Y.; Kyuwa, S.; Yoshikawa, Y., Age-related changes of intracellular A beta in cynomolgus monkey brains. *Neuropathol. Appl. Neurobiol.* **2005,** 31, (2), 170-180.

73. Klyubin, I.; Walsh, D. M.; Lemere, C. A.; Cullen, W. K.; Shankar, G. M.; Betts, V.; Spooner, E. T.; Jiang, L. Y.; Anwyl, R.; Selkoe, D. J.; Rowan, M. J., Amyloid beta protein immunotherapy neutralizes A beta oligomers that disrupt synaptic plasticity in vivo. *Nat. Med. (N. Y., NY, U. S.)* **2005,** 11, (5), 556-561.

74. Thakker, D. R.; Weatherspoon, M. R.; Harrison, J.; Keene, T. E.; Lane, D. S.; Kaemmerer, W. F.; Stewart, G. R.; Shafer, L. L., Intracerebroventricular amyloid-beta antibodies reduce cerebral amyloid angiopathy and associated micro-hemorrhages in aged Tg2576 mice. *Proc. Natl. Acad. Sci. U. S. A.* **2009,** 106, (11), 4501-4506.

75. Sarroukh, R.; Cerf, E.; Derclaye, S.; Dufrêne, Y.; Goormaghtigh, E.; Ruysschaert, J.-M.; Raussens, V., Transformation of amyloid β(1–40) oligomers into fibrils is characterized by a major change in secondary structure. *Cell. Mol. Life Sci.* **2011,** 68, (8), 1429-1438.

76. Greenfield, N. J., Using circular dichroism spectra to estimate protein secondary structure. *Nat. Protoc.* **2006,** 1, (6), 2876-90.

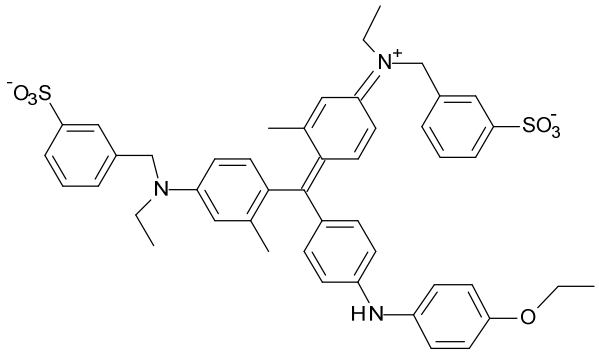

Brilliant Blue G (BBG)

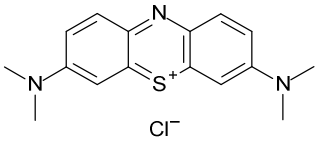

Methylene Blue (MB)

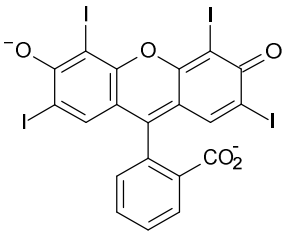

Erythrosine B (ER)

Figure 1. Chemical structure of brilliant blue G (BBG), methylene blue (MB), and erythrosine B (ER) at neutral pH.

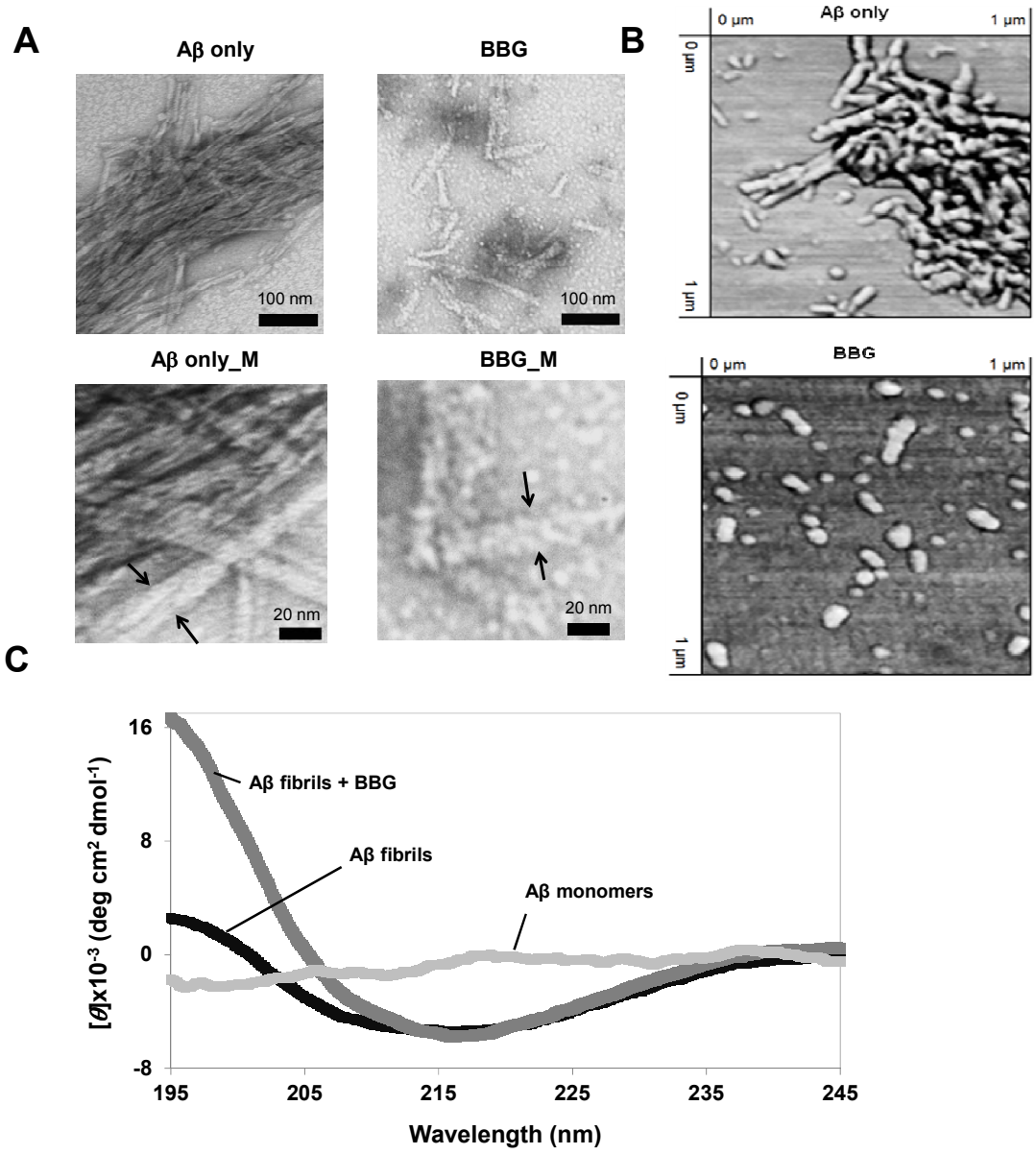

Figure 2. Properties of the Aβ fibrils incubated in the absence or presence of BBG. TEM (A) and AFM images (B, 1x1 μm) of the Aβ fibrils incubated for one day in the absence of any dye (Panel Aβ only) or presence of 10x BBG (Panel BBG). The sections of the two TEM images were magnified (Panels Aβ only_M and BBG_M). Each pair of arrows illustrates the width of the Aβ aggregates. TEM scale bar is 100 nm (Top Panels) or 20 nm (Bottom Panels). (C) CD spectra of Aβ monomers, Aβ fibrils incubated in the absence (Aβ fibrils) or presence of 10x BBG (Aβ fibrils + BBG) for one day.

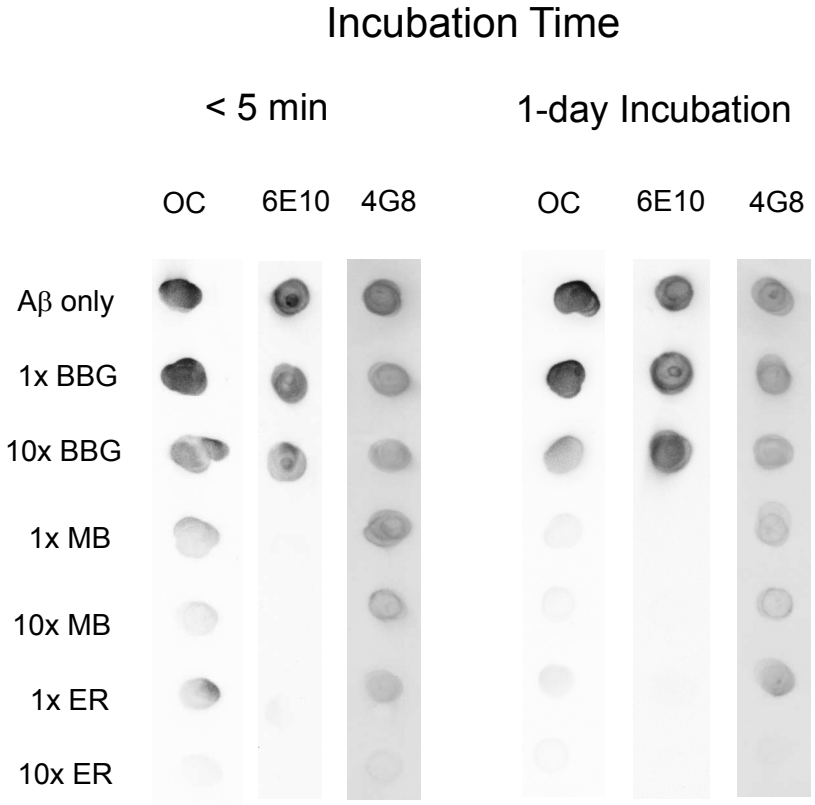

Figure 3. Dot-blot images of the Aβ fibrils incubated in the absence (Aβ only) or presence of 1x and 10x BBG, MB, or ER for less than 5 minutes (Panel < 5 min) or one day (Panel 1-day incubation). For each antibody, all samples were spotted onto the same nitrocellulose membrane. Each membrane was immuno-stained with the OC, 6E10, or 4G8 antibody. For clearer presentation of the data, the sections of each membrane were cut and re-arranged.

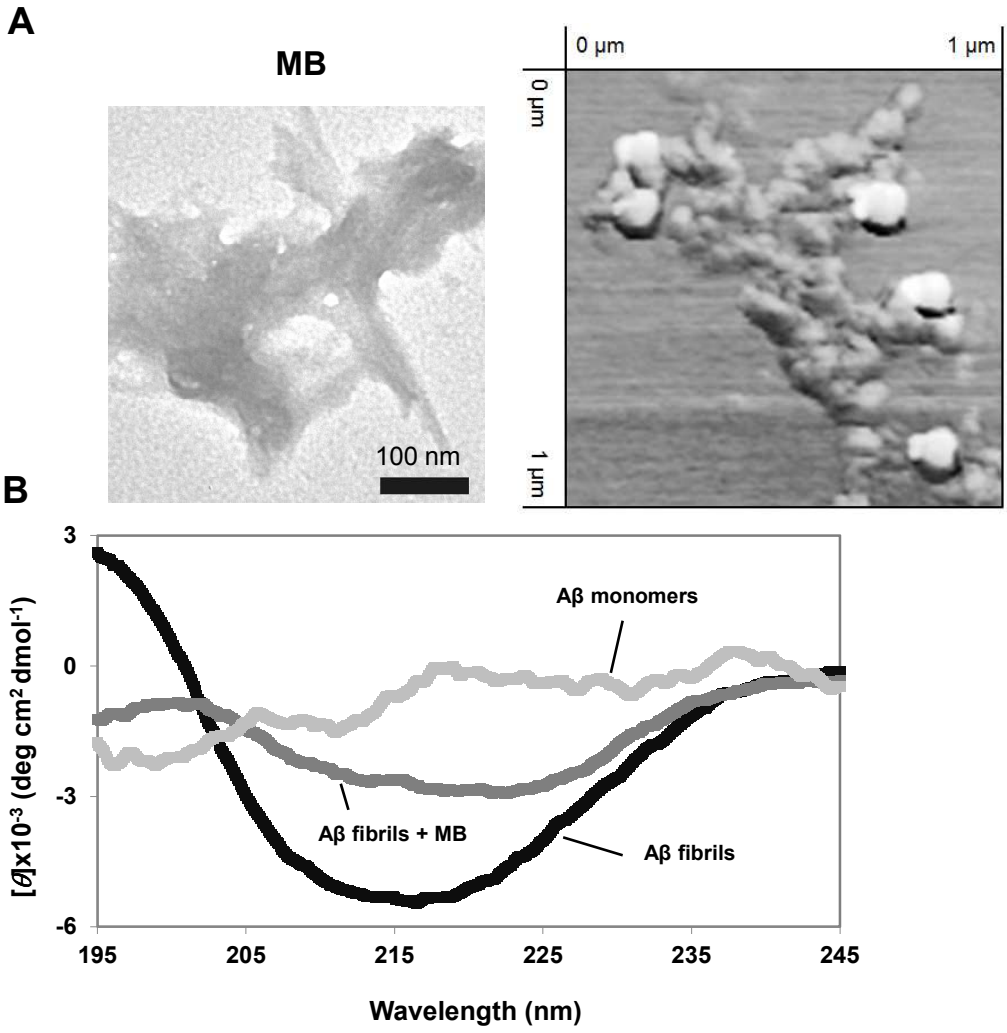

Figure 4. Properties of the Aβ fibrils incubated in the absence or presence of MB. (A) TEM (left panel) and AFM (right panel, 1x1 µm) images of the Aβ fibrils incubated for one day in the presence of 10x MB. TEM scale bar is 100 nm. (B) CD spectra of Aβ monomers, Aβ fibrils incubated in the absence (Aβ fibrils) or presence of 10x MB (Aβ fibrils + MB) for one day.

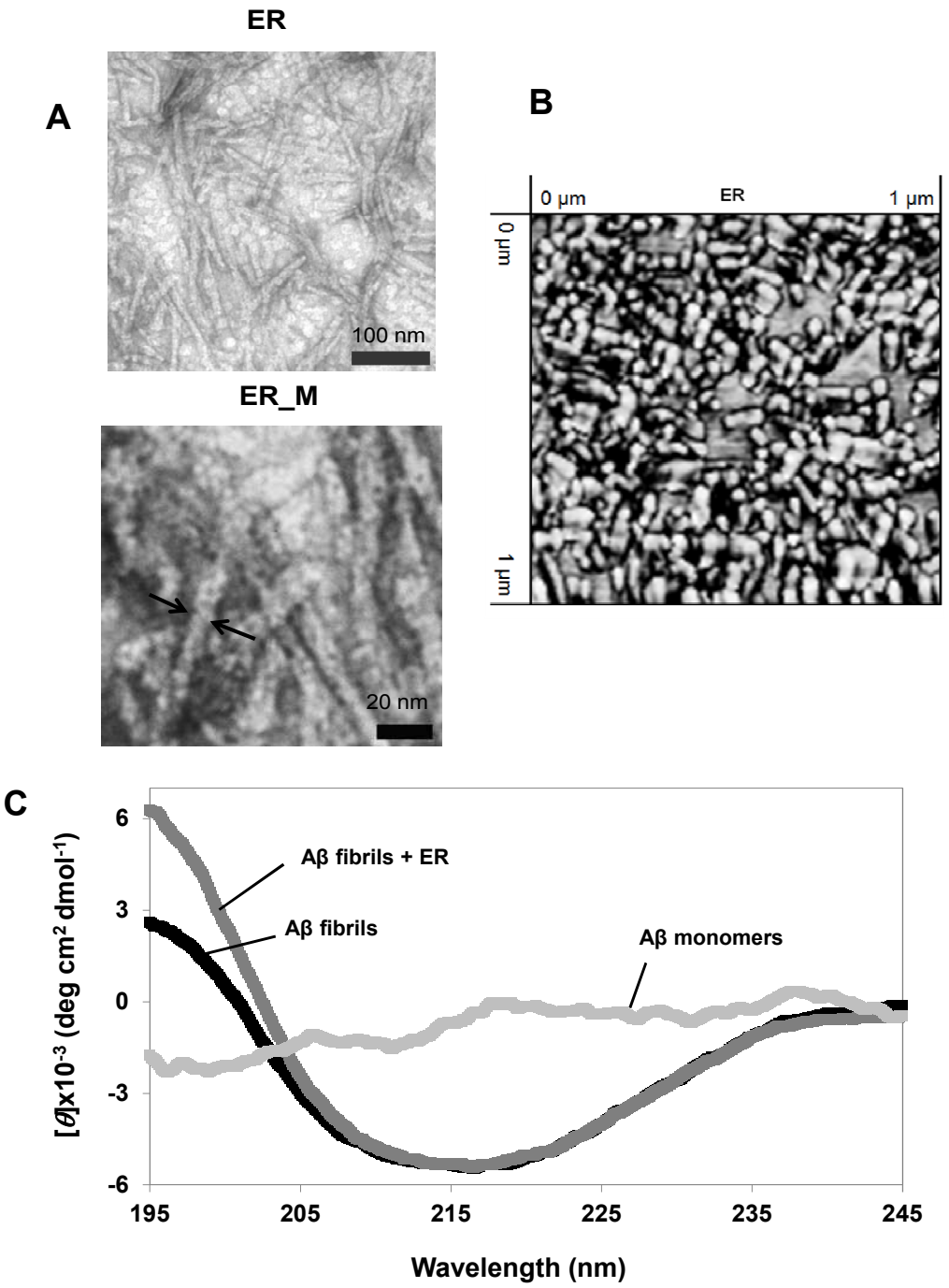

Figure 5. Properties of the Aβ fibrils incubated in the absence or presence of ER. TEM (A) and AFM (B, 1x1 µm) images of the Aβ fibrils incubated for one day in the presence of 10x ER (Panel ER) and the magnified section (Panel ER_M). The pair of arrows illustrate the width of the Aβ aggregates. TEM scale bar is 100 nm (Panel ER) or 20 nm (Panel ER_M). (C) CD spectra of Aβ monomers, Aβ fibrils incubated in the absence (Aβ fibrils) or presence of 10x ER (Aβ fibrils + ER) for one day.

Table 1: Measured[a] TEM length (A) and width (B) distribution[b] of Aβ fibrils incubated in the presence or absence of 10X BBG and 10X ER for one day at 37◦C.

A.

	Length of Aβ Aggregates (μm)												
	0.1	0.2	0.3	0.4	0.5	0.6	0.7	0.8	0.9	1	1.1	>1.1	Average (nm)
Fibrils Only	ND	2%	4%	8%	10%	10%	6%	10%	4%	2%	10%	35%	1026 ± 621
10X BBG	34%	54%	9%	3%	ND	ND	ND	ND	ND	ND	ND	ND	133 ± 65
10X ER	3%	18%	32%	32%	9%	3%	2%	1%	ND	ND	ND	ND	303 ± 129

B.

	Width of Aβ Aggregates (nm)													
	6	8	10	12	14	16	18	20	22	24	26	28	>28	Average (nm)
Fibrils Only	ND	ND	ND	2%	10%	10%	25%	13%	21%	10%	4%	4%	1%	19 ± 4
10X BBG	ND	ND	ND	ND	ND	1%	10%	4%	10%	11%	19%	8%	37%	26 ± 7
10X ER	1%	7%	48%	25%	17%	2%	ND	ND	ND	ND	ND	ND	ND	10 ± 2

[a]Measured using Image J software.

[b]The aggregate length or width bin labels represent the maximum length or width of aggregates in each respective bin. Shown on the table are the proportions of each sample population measured possessing the respective maximum bin length or width. Minimum one hundred aggregates except fifty one fibrils only aggregates for length distribution were used to obtain the distribution.

ND: Not Detected

Table 2: Secondary structure content[a] of Aβ fibrils incubated[b] in the absence or presence of BBG or ER.

Dye added[c]	α-helix	β-sheet	β-turn	Disordered
-	12.2%	36.4%	12.1%	39.3%
BBG	12.8%	44.4%	9.9%	32.9%
ER	12.7%	36.8%	11.8%	38.6%

[a] Determined by DichroWeb using CONTIN method and SP175 reference proteins

[b] Incubated at 37 ˚C without shaking for one day.

[c] Aβ:small molecule (BBG or ER) = 1:10 molar ratio

Table 3: Secondary structure content[a] of Aβ fibrils incubated[b] in the absence or presence of MB.

Small molecule added[c]	α-helix	β-sheet	β-turn	Disordered
-	10.1%	32.2%	27.4%	30.3%
MB	8.4%	18.3%	4.3%	69.0%

[a] Determined by DichroWeb using CONTIN method and Set 6 reference proteins

[b] Incubated at 37 °C without shaking for one day.

[c] Aβ:MB = 1:10 molar ratio

For Table of Contents Use Only

Different Fates of Alzheimer's Disease Amyloid-beta Fibrils Remodeled by Biocompatible Small Molecules

Jacob A. Irwin, H. Edward Wong, Inchan Kwon